

# Difference Image Analysis of Galactic Microlensing

## II. Microlensing Events

C. Alcock<sup>1,2</sup>, R.A. Allsman<sup>3</sup>, D. Alves<sup>1,4</sup>, T.S. Axelrod<sup>5</sup>, A.C. Becker<sup>6</sup>, D.P. Bennett<sup>1,2</sup>, K.H. Cook<sup>1,2</sup>, A. J. Drake<sup>5</sup>, K.C. Freeman<sup>5</sup>, K. Griest<sup>2,7</sup>, M.J. Lehner<sup>8</sup>, S.L. Marshall<sup>1,2</sup>, D. Minniti<sup>1,13</sup>, B.A. Peterson<sup>5</sup>, M.R. Pratt<sup>9</sup>, P.J. Quinn<sup>10</sup>, C.W. Stubbs<sup>2,5,6</sup>, W. Sutherland<sup>11</sup>, A. Tomaney<sup>6</sup>, T. Vandedei<sup>7</sup>, and D.L. Welch<sup>12</sup>

(The MACHO Collaboration)

### ABSTRACT

The MACHO collaboration has been carrying out Difference Image Analysis (DIA) since 1996 with the aim of increasing the sensitivity to the detection of gravitational microlensing. This is a preliminary report on the application of DIA to galactic bulge images in one field.

We show how the DIA technique significantly increases the number of detected lensing events, by removing the positional dependence of traditional photometry schemes and lowering the microlensing event detection threshold. This technique, unlike PSF photometry, gives the unblended colours and positions of the microlensing source stars. We present a set of criteria for selecting microlensing events from objects discovered with this technique. The 16 pixel and classical microlensing events discovered with the DIA technique are presented.

*Subject headings:* Cosmology: gravitational lensing - methods: data analysis - Galaxy: stellar content; center - stars: brown dwarfs

---

<sup>1</sup>Lawrence Livermore National Laboratory, Livermore, CA 94550

<sup>2</sup>Center for Particle Astrophysics, University of California, Berkley, CA 94720

<sup>3</sup>Supercomputing Facility, Australian National University, Canberra, ACT 0200, Australia

<sup>4</sup>Department of Physics, University of California, Berkeley, CA 95616

<sup>5</sup>Mount Stromlo and Siding Spring Observatories, Weston Creek, Canberra, ACT 2611, Australia

<sup>6</sup>Department of Astronomy and Physics, University of Washington, Seattle, WA 98195

<sup>7</sup>Department of Physics, University of California, San Diego, CA 92093

<sup>8</sup>Department of Physics, University of Sheffield, Sheffield s3 7RH, UK

<sup>9</sup>Center for Space Research, MIT, Cambridge, MA 02139

<sup>10</sup>European Southern Observatory, Karl Schwarzschild Str. 2, D-85748 Gärching bel München, Germany

<sup>11</sup>Department of Physics, University of Oxford, Oxford OX1 3RH, UK

<sup>12</sup>Department of Physics and Astronomy, McMaster University, Hamilton, ON L8S 4M1, Canada

<sup>13</sup>Departamento de Astronomia, P. Universidad Católica, Casilla 104, Santiago 22, Chile

## 1. INTRODUCTION

The on-going search for microlensing events in the direction of the galactic bulge is now reaching its prime with over 300 events detected by the MACHO (Alcock et al. 1998a), EROS (Beaulieu et al. 1995), DUO (Alard & Guibert 1997) and OGLE (Paczynski et al. 1994) groups.

Microlensing research in the bulge, although initially only a test-bed for the phenomenon of microlensing, has now graduated to become an area for study in its own right. These microlensing events allow us to study the atmospheres of clump giants in the bulge (Alcock et al. 1997b; Heyrovsky et al. 1999), and possibly detect the existence of distant extra-solar planets (Griest and Neda 1998; Becker et al. 1998). The optical depth determined from the events permit us to calculate the number density and masses of objects intervening between us and the source stars. The spatial distribution of these events will help in determining the distribution of mass within our galaxy. Aside from the benefits from the microlensing to the astronomical community, there are other important uses of the years of observations of millions of stars. For instance, within the datasets there are years of coverage of thousands of variable stars, see for example (Alcock et al. 1997c, 1998b).

In this initial Difference Image Analysis (hereafter DIA) study, we once again use the bulge as a test-bed for microlensing analysis. As before, we use the bulge as a target because of the large number of microlensing events observed toward the bulge relative to the LMC. We perform the DIA technique in an attempt to increase our efficiency for detecting microlensing events. With the successful result of increasing the detection rate of microlensing towards the bulge, we can now be optimistic about applying it on data taken towards the LMC, where the present number of detected events is small.

In the §3 we will present the microlensing events found in this analysis. In §4 and §5 we will analyse these new results. In the final section we shall make our concluding remarks about the results and potential of the technique.

## 2. OBSERVATIONS

This analysis presents results from the application of the DIA technique on 324 observations of a single  $42'$  by  $42'$  field centred at  $\alpha = 18^{\circ}01'20''$ ,

$\delta = -28^{\circ}17'39''$  ( $J2000$ ). Observations were taken on the Mount Stromlo and Siding Spring Observatories' 1.3m Great Melbourne Telescope with the dual-colour 4k by 4k *Macho camera*. All bulge observations have 150 second exposures. See Alcock et al. 1999a for further details.

*The data analysis strategy and details of the DIA technique are presented in paper I (Alcock et al. 1999a).*

## 3. RESULTS

The result of the analysis carried out on three years of bulge data for an individual field is the detection of thousands of variables, over a hundred asteroids and 16 probable microlensing events. Of which nine events are classified as classical events and seven as pixel lensing events. Classical microlensing involves resolved source stars. Pixel lensing involves source stars which are too faint or too blended to be resolved. A typical difference image is shown on the right of figure 1, where the reference image is presented on the left.

Of the 324 observations put through the bulge DIA pipeline 306 observations were successfully reduced. This constitutes  $\sim 80\%$  of the original data set of observations for this field. The 18 reduction failures in the analysis occurred due to poor data conditions. This included bad geometric registration due to saturated registration stars and very low transmission relative to the reference image (as low as 15% reference image flux).

### 3.1. Event Selection

The search for microlensing events is simplified by the fact that the template is created by the combination of multiple images over a long time baseline. Most variables in the constituent images are thus observed at a range of phases making the reference image close to an average phase for each variable. This means that a large percentage of variable stars will have positive and negative excursions from their mean amplitude. However, microlensing events and asteroids will generally only have excursions above the baseline. This property allows us to considerably reduce the size of the search by only investigating results with positive excursions from the median baseline. This selection means it is quite possible that we could miss events which have long time scales ( $\dot{t} \gtrsim 1$  year).

To perform event selection one must realise that spurious detections of objects can occur for a number of reasons. The most common sources of these are asteroids, satellite tracks and cosmic rays. Numerous detections of cosmic rays occur, but these are removed in the process of matching object positions in two colours. Asteroids and satellite tracks are detected in two colours and are thus more difficult to remove from an individual observation. To rule out these detections the search for microlensing detections must be made with at least two consecutive significant detections in two colours, at any given position. However, one can not determine the time scale  $\hat{t}$  or the amplification  $A$  for microlensing events which are detected from only two consecutive points above the baseline in a light curve. Such results can also sometimes be caused by poor photometry due to bad seeing or CCD defects. For this reason we searched the photometric database for events of at least 4.5 sigma significance in at least three consecutive observations. This significantly lowered the number of short time scale events we expected to detect. For this data set the cuts led to a microlensing time scale ( $\hat{t}$ ) lower limit of approximately five days.

Events with a lower signal-to-noise ratio (hereafter S/N) are selected based on 4 or more consecutive points. In all cases an event must have a total S/N of greater than ten in each colour. Each of these so called *point filters* require a positive deviation from baseline (median) in consecutive observations of an object. These point filters have the effect of reducing the number of possible events to roughly 15% of the initial data set.

DIA sometimes deals with variable objects of an indeterminate magnitude, so a set of cuts different from those used previously in Alcock et al. (1997a) was imposed. Variable stars detected in this analysis were cut in the selection process with a number of variable star point filters. For example, if there are four or more consecutive points 3.5 sigma below the median, the result is deemed to be due to a variable star. Such a result is not consistent with microlensing and is too significant to be due to poor photometry alone.

Observations of bulge fields are generally only taken once per night for approximately eight months of the year. This means a large number of bulge events are missed because they occur during the observing gap. A number of possible events are detected as rising at the end of the observing season, or falling

at the beginning of the next. But these events can be ambiguous. For such events it is sometimes difficult to obtain useful parameters from light curve fitting if we do not know the maximum flux of the event. We therefore require the maximum amplification occurs during the time the object was monitored.

In our cuts we do not require the microlensing light curve has a single peak as is common with many sets of cuts. Not applying this type of cut makes the removal of variables more difficult, but allows us to detect binary lensing events where multiple peaks are apparent. Further cuts based on the microlensing fit were also applied. But these cuts also do not remove binary events from the list of detected objects (see below). All light curves passing the first cuts stage were examined before this cut was applied.

With DIA we do not necessarily know the true baseline magnitude of the objects. So in contrast to Alcock et al. (1997a) we do not impose an amplitude threshold cut for microlensing events. Furthermore, since DIA is not affected by source crowding, we made no cut for this either. This initial set of variable cuts reduced the number of results from  $\sim 9000$  to 80.

Most of the points in the light curve of a microlensed star should lie near the median baseline and be consistent with a microlensing fit. So the remaining light curves next underwent fitting for microlensing and for a constant baseline outside the microlensed region. A second set of cuts is then performed based on the  $\chi^2$  values from these fits to remove the remaining low amplitude variables.

We selected events with microlensing fit  $\chi_m^2 < 2.5$  and constant baseline fit  $\chi_c^2 < 6$  in the region  $t_0 \pm 2\hat{t}$ .  $\chi_m^2$  and  $\chi_c^2$  are the reduced chi-squared statistics of the fits. Microlensing events can vary significantly from a point source microlensing fit (e.g. events with parallax). For microlensing events we require  $1000/pf \times (\chi_c^2 + \chi_m^2) < 3.6$ , where  $pf$  is flux at peak amplification in ADU. This selection acts as a S/N cut for the detected events. For events with a peak flux greater than 25000 ADU, we do not require the microlensing cut or the baseline constancy cut. These events generally have a high S/N, but may not pass our simple microlensing  $\chi^2$  fit cut because of structure. The event 97-BLG-28 (next section) falls into this category because of the caustic crossing. For these events we required a more stringent signal to noise cut of  $1000/pf \times (\chi_c^2 + \chi_m^2) < 1.5$ . The final cut we imposed on all events was that the microlensing fit colour be greater than  $V - R = 0.55$ . This cut

removes dwarf novae which can be quite well fitted by a microlensing in some cases, but are much bluer during outburst.

The effect of these  $\chi^2$  cuts on the 80 events passing the variable cuts is shown in figure 3. One can see that most of the events which fail the constant background cut also fail the microlensing fit cut. This demonstrates the robustness of this set of cuts.

### 3.2. Parameters of Microlensing Events

The parameters for the sources of candidate microlensing events are given in table 1, with difference image photometry colours  $(V - R)_d$  and those of the nearest matching MACHO database object  $(V - R)_p$ . The extinction corrected source colours  $(V - R)_{c0}$  are also given. The difference image source coordinates and the separation  $S$  of the nearest database object are presented. Events which were alerted on are noted.

We have used the Starlink software package *Astrom* to perform astrometry on the coordinates of difference image objects to determine the RA and Dec of sources. The nearest matching Macho database stars were found using their coordinates and the results are presented. The associated errors in  $S$  are mainly due to the uncertainty in the transformation between difference image template and the pipeline photometry template.

The V-R colours in this table were obtained by the standard Macho calibrations (Alves 1998). The Cousins magnitudes for the bulge are given by:

$$V_c = 23.67 + 0.847 \times B_m + 0.156 \times R_m \quad (1)$$

$$R_c = 23.48 + 0.822 \times R_m + 0.182 \times B_m \quad (2)$$

Here  $B_m$  and  $R_m$  are the Macho camera blue and red passbands, respectively. Extinctions have been determined from RR Lyrae stars in the proximity of microlensing events. For RR Lyrae stars we have used  $E_{V-R} = (V - R)_{obs} - 0.21$  (Alcock et al. 1998a). Using the standard extinction law of Rieke and Lebofsky (1985), we obtain  $A_v = 3.96E(V - R)$ .

As the differential reddening in this field is large (Alcock et al. 1998a), we chose to extinction correct each event individually based on the RR Lyrae within  $1'$ . This technique has some uncertainty because of

the small numbers of RR Lyrae in each field. In future we hope to use the more numerous red clump giant stars to determine extinctions more accurately. The consistency of these two methods has recently been demonstrated for Baades window by Alcock et al. (1998b) and Gould et al. (1998a). The difference image colours of the events come from stacking the images over the period where the event was two sigma above the detection threshold. This gives accurate colours for events which are independent of any blending in the template. PSF photometry colours have been determined from the baseline colours of the Macho objects. The difference between these colours and the DIA colour can be seen in figure 2. This shows the extent of blending for these sources. Points are shown with one sigma uncertainties.

## 4. EVENTS

The number of alert events which pass our selection cuts for the period of this reduction is eight and the number of new possible microlensing events is also eight.

All the events detected in this analysis were fit with a point source point lens microlensing fit. The values are given in table 2 for classical results and in table 3 for pixel lensing. Plots of the fits are given in figures 4 and 5. Two binary microlensing events which have not been fit are given in figure 6. For most of these events there is insufficient sampling to accurately determine the source flux. Therefore we have chosen to use the measured reference image baseline flux as the maximum flux which can be contributed by the source. This gave us a limit on the minimum amplification  $A_{min}$  and time scale of the event  $\hat{t}_{min}$ . In a future paper (Alcock et al. 1999c) we shall use HST data of the bulge to determine luminosity function for this and other fields. This will enable us to determine detection efficiencies for events due to source stars several magnitudes below the crowding limit of this data.

We shall now briefly discuss the individual microlensing candidates. Events 95-BLG-33, 95-BLG-32 and 95-BLG-38 are classified as excellent microlensing candidates. Event 95-BLG-21 has an excess of flux at peak amplitude which could be due to the source passing near a caustic. However, this candidate is a excellent microlensing candidate event. Event 95-BLG-14 is a good microlensing candidate, although there are a few missing data points in the blue passband due

to a CCD defect near the source position. Event 96-BLG-16 has a poor  $\chi^2$  in the PSF photometry due to the fact that this source is highly blended. The fit parameters for this event (table 2) are different from those given in figure 7 of paper I as the baseline flux is fixed for fits in figure 4. In figure 7 of paper I the source flux has been fit for. Candidate 97-BLG-28 is a poor fit to single point source microlensing because there is a cusp crossing near maximum amplification. Still this event is regarded as an excellent microlensing candidate. A thorough analysis of this event will be presented in a future paper (Alcock et al. 1999b). Event 97-BLG-51 is an example of a moderate signal lensing event. Although the light curves do not extend far past maximum light, further points available in the PSF photometry reduction give further weight. The discrepancy in the two fit amplitudes is due to the fact that the PSF photometered star is not the lensed star, but rather, is a nearby star sequestering some of the light in the PSF photometry.

Events 95-BLG-d2, 95-BLG-d3, 95-BLG-d4, 95-BLG-d5, 97-BLG-d1 and 97-BLG-d3 are all good candidate microlensing events. Here the use of a *d* before the final number means the event was first discovered in the difference image analysis. The amplification values for 95-BLG-d5, 95-BLG-d3 and 97-BLG-d1, are all quite low but it should be mentioned that these are the minimum possible amplitudes. Event 96-BLG-d1 is reasonably fit with a microlensing light curve though it appears to have a feature on the rising side. This feature could be the signature of a binary microlensing event and is considered a good candidate microlensing event. Event 97-BLG-d2 is a very poor point source lensing event but is a very good candidate binary lensing event. This event will be subjected to a detailed analysis in a future paper (Alcock et al. 1999c).

Possible cases of the detection of pixel lensing have been presented in the past (Crotts & Tomaney 1997). However, it is believed their survey suffered from insufficient baseline to rule variable stars out as the sources (Gould & Depoy 1998b). Of the new DIA results presented here, six are probably pixel lensing events, based on their nearest resolved star separations and colours and light curves. These are 95-BLG-d2, 96-BLG-d1, 97-BLG-d1, 97-BLG-d2, 97-BLG-d3 and 95-BLG-d4. The other two good candidate events (95-BLG-d3, 95-BLG-d5) are probably classical microlensing events which fall below the PSF photometry alert system detection threshold (Alcock et al.

1999b).

## 5. SUMMARY

We have shown how the DIA technique can be used on archival data to detect microlensing events undetected with the traditional approach. This is achieved by removing the positional constraints and accurately removing non-variable objects. Nine classical microlensing events and seven pixel lensing events were found. Of these results, eight events were new events undetected by the alert system.

DIA is unaffected by unlensed blended flux. Because of this, it is possible to determine the existence of a blending even where the separation between source and blended flux centroid is small, by comparing DIA colours with PSF photometry colours. Our results prove that it is possible to determine the source flux from DIA light curves for bright sources and hence obtain accurate  $\hat{t}$  values for such events. The first pixel lensing candidates with sufficiently long baselines to prove their existence have been presented.

Three methods for determining useful parameters from difference image results have been presented. Firstly for high S/N events, we can fit for the source flux of the event to obtain  $\hat{t}$ . For lower S/N results we can impose the flux in the reference as a upper bound and obtain a limit on  $\hat{t}$ . Lastly from paper I, we can use a deep colour magnitude diagram (such as HST) to determine the distribution of source stars colours with magnitude. With this and the colour of the source, and its associated uncertainties, we can determine a distribution of allowable  $\hat{t}$  values. This in turn could provide us with a  $\hat{t}$  distribution for the set of events.

In future, DIA will allow us to gain greater sensitivity to detecting long time scale low amplification events. The detection of these events will be accomplished by simply stacking difference images to increase the detectable signal of these events. For such events parallax can be measured and used to break the degeneracy in lens mass and position.

We are grateful for the skilled support by the technical staff at Mount Stromlo Observatory. Work at Lawrence Livermore National Laboratory is supported by DOE contract W7405-ENG-48. Work at the center for Particle Astrophysics at the University of California, Berkeley is supported by NSF grants AST 88-09616 and AST 91-20005. Work at Mount

Stromlo and Siding Spring Observatories is supported by the Australian Department of Industry, Technology and Regional Development. Work at Ohio State University is supported in part by grant AST 94-20746 from the NSF. W. J. S. is supported by a PPARC Advanced Fellowship. K. G. is grateful for support from DOE, Sloan, and Cottrell awards. C. W. S. is grateful for support from the Sloan, Packard and Seaver Foundations. This work was carried out by A.J.D. in partial fulfilment of the requirements for the degree of PhD at ANU.

## REFERENCES

- Alard, C., & Guibert, J. 1997, *A&A*, 326, 1
- Alcock, C., et al. 1997a, *ApJ*, 479, 119
- Alcock, C., et al. 1997b, *ApJ*, 491, 436
- Alcock, C., et al. 1997c, *ApJ*, 474, 217
- Alcock, C., et al. 1998a, *ApJ*, 492, 190
- Alcock, C., et al. 1998b, *ApJ*, 492, 190
- Alcock, C., et al., 1999a, In preparation
- Alcock, C., et al., 1999b, In preparation
- Alcock, C., et al., 1999c, In preparation
- Alves, D. 1998, PhD thesis
- Beaulieu, J. P., et al. 1995, *A&A*, 299, 168
- Becker, A. C., et al. 1998, *BAAS*, 193, 108.5
- Crotts, A., Tomaney, A. 1997, *ApJ*, 473, L87
- Gould, A., et al. 1998, *ApJ*, 492, 778
- Gould, A., & Depoy D. L., 1998, *ApJ*, 497, 62
- Griest, K. & Neda S. 1998, *ApJ*, 500, 37
- Heyrovsky, D., Sasselov D. & Loeb A. 1999, *astro-ph* 9902273
- Paczyński, B., et al. 1994, *A&AS*, 187, 14.07
- Rieke, G. H., & Lebofsky, M. J. 1985, *ApJ*, 288, 618

Fig. 1.— Results of the DIA reduction. Left: A ( $250'' \times 500''$ ) section of a reference image. Right: a difference image of the same section. A number of variables are clearly visible. Plain grey regions in the difference frame correspond to areas masked during reduction because of saturation and bad columns in the test image.

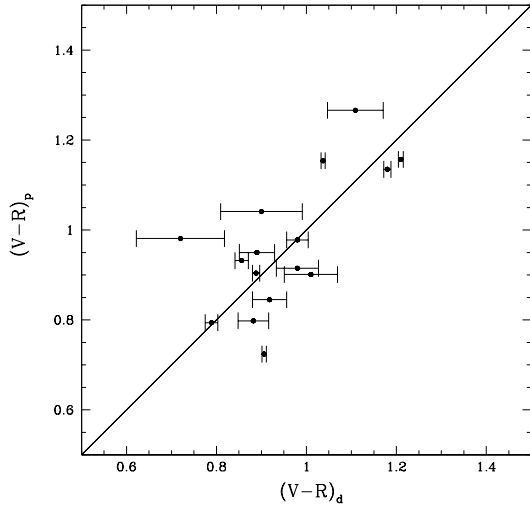


Fig. 2.— The colours of microlensing sources determined from PSF photometry, compared to the colours of the same sources determined from difference images. The offsets from the diagonal line come from blending of the PSF colours. Errors in the PSF photometry baselines are negligible and so are not shown, see table 1.

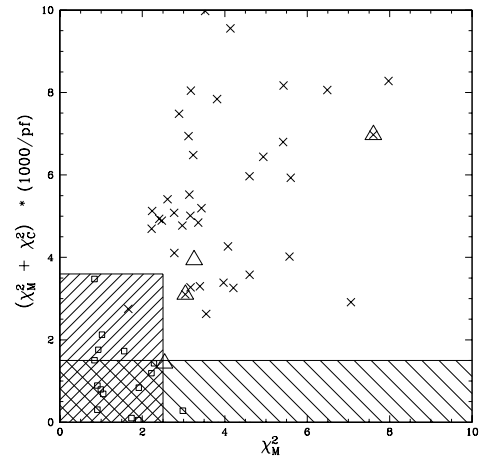


Fig. 3.— Two sets of cuts performed on microlensing candidates which passed the variability cuts. Microlensing events with flux at maximum amplification is greater than 25000 ADU must lie in the ‘\’ hatched region. Events with flux at maximum amplification is less than 25000 ADU must lie in the ‘/’ hatched region. For specifics see the text. Here the  $\times$  symbols represent results which fail the constant baseline cut, triangles those which fail the V-R colour cut and squares the events which pass all cuts. One microlensing event which passes these cuts lies outside the region displayed in this figure.

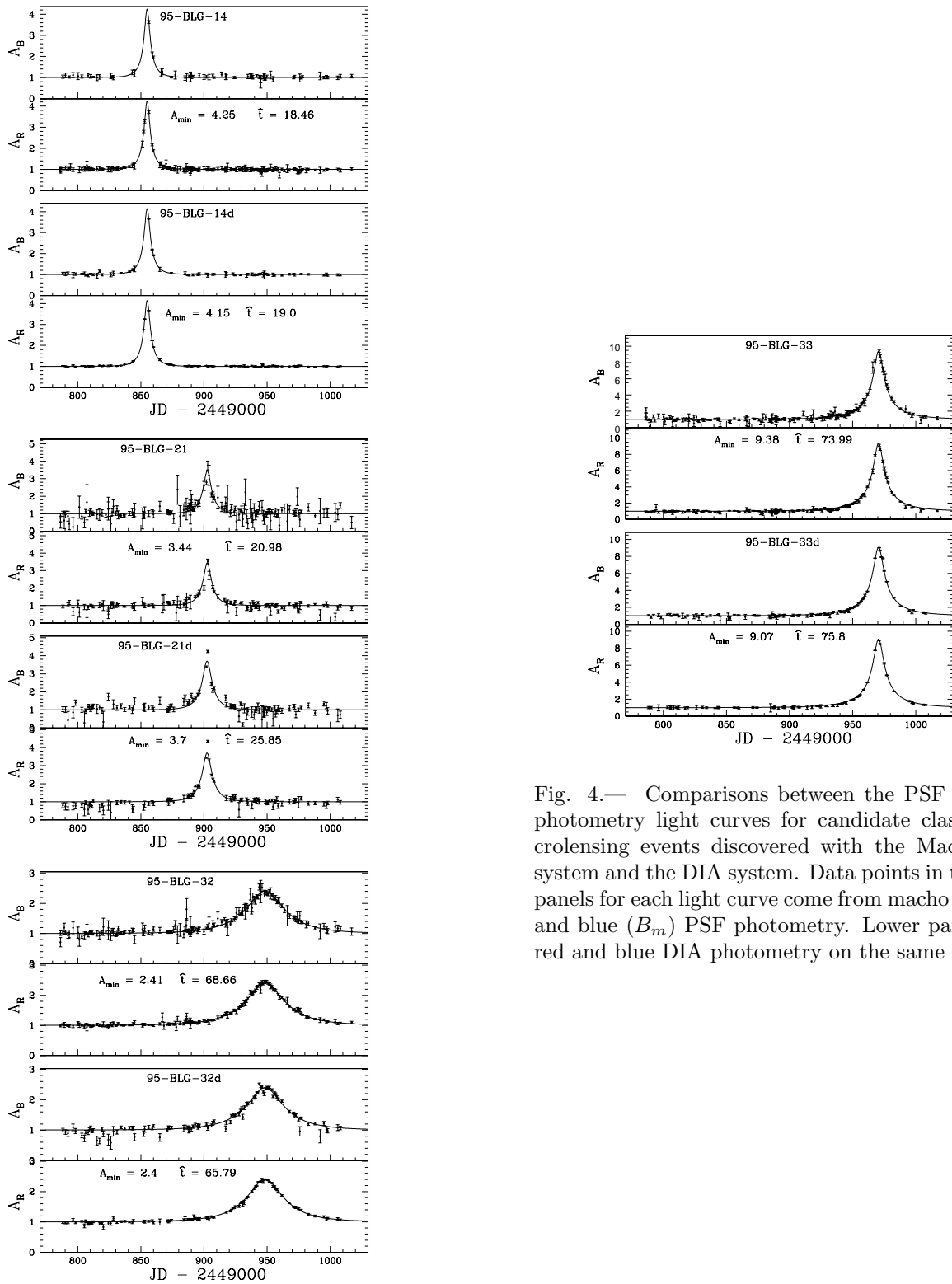


Fig. 4.— Comparisons between the PSF and DIA photometry light curves for candidate classical microlensing events discovered with the Macho Alert system and the DIA system. Data points in the upper panels for each light curve come from macho red ( $R_m$ ) and blue ( $B_m$ ) PSF photometry. Lower panels from red and blue DIA photometry on the same images.



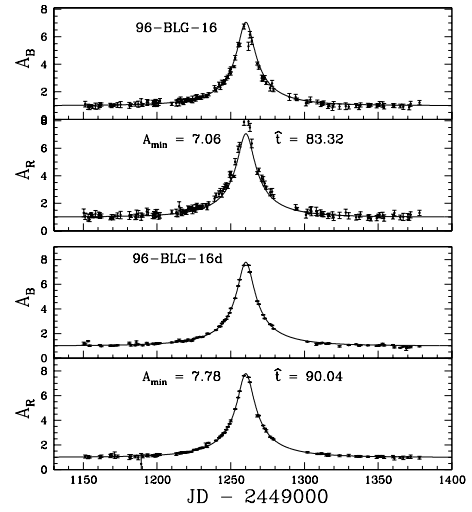
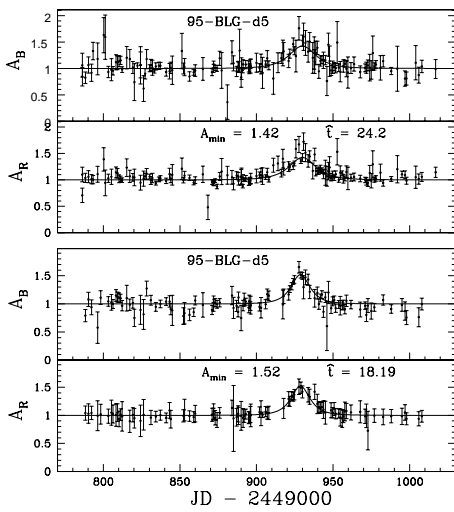
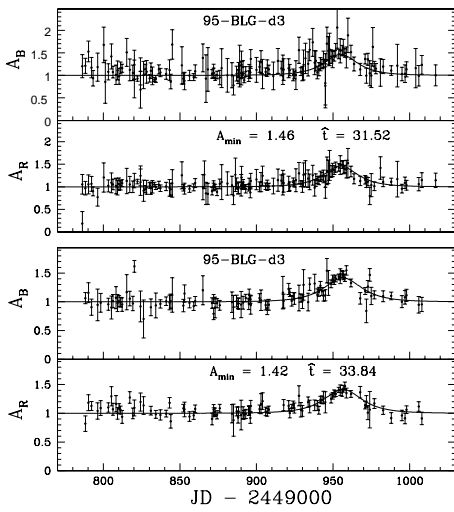
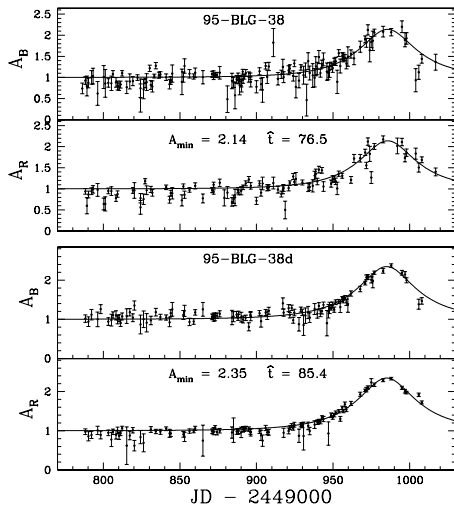


Fig. 4.— *continued*

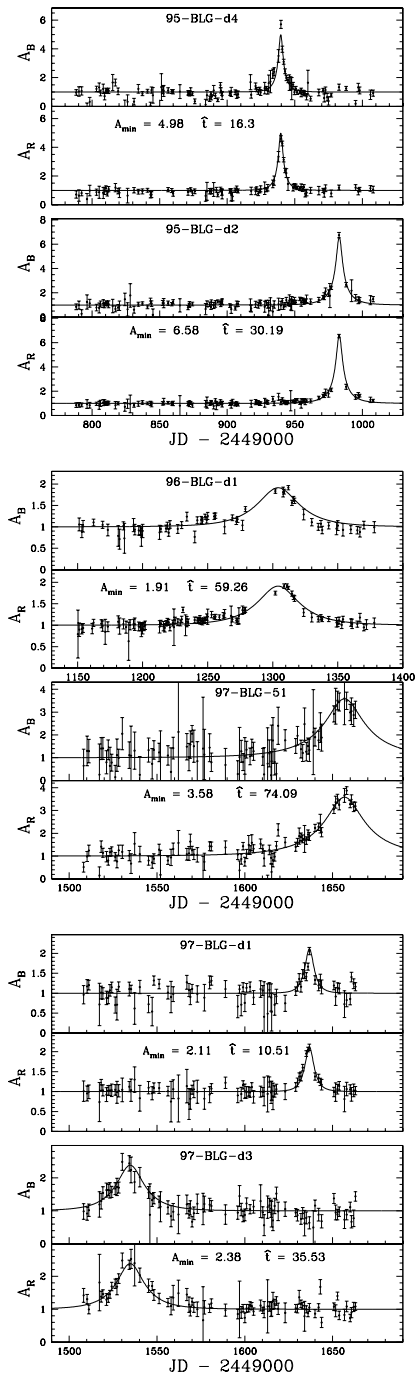


Fig. 5.— This figure shows light curves of candidate pixel microlensing events discovered with the DIA analysis. Upper panels are from the blue passband, lower panels are from red band photometry.

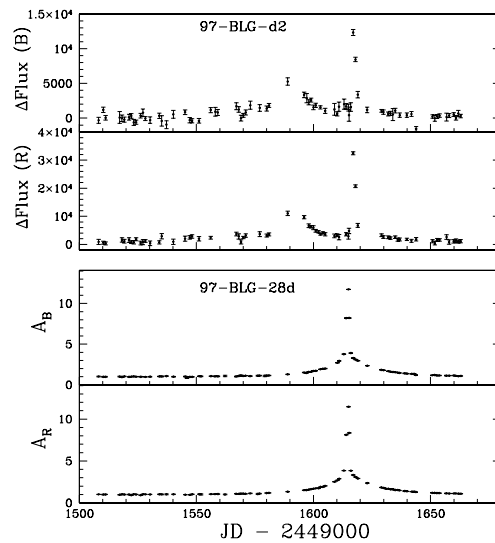


Fig. 6.— The two binary microlensing events discovered in this analysis. The top two panels contain a candidate binary pixel lensing event. Here the baseline flux is unknown so difference flux is plotted instead of  $A$ . The lower panels contain an event with a cusp crossing discovered by the Macho alert system. The fits for these events will be presented in later work (Alcock et al. 1999b).

TABLE 1  
PARAMETERS OF EVENTS.

Event (1)	R.A. (2000) (2)	Decl. (2000) (3)	V (4)	(V-R) <sub>p</sub> (5)	(V-R) <sub>d</sub> (6)	(V-R) <sub>rr</sub> (7)	(V-R) <sub>c0</sub> (8)	S (") (9)	Alert (10)
95 BLG 33	18 01 57.1	-28 08 06	19.14	1.152(3)	1.037(5)	0.89(5)	0.397(50)	0.16(0.2)	y
95 BLG d2	18 01 13.8	-28 01 25	20.13	1.041(6)	0.900(91)	0.80(5)	0.350(60)	0.53(0.3)	n
97 BLG 28	18 00 33.8	-28 01 10	18.10	1.155(1)	1.210(5)	0.83(5)	0.640(50)	0.12(0.2)	y
97 BLG 51	18 00 39.3	-27 58 35	20.56	0.915(7)	0.980(47)	0.74(6)	0.49(10)	0.79(0.5)	y
96 BLG d1	18 00 36.1	-27 58 30	19.41	0.901(4)	1.010(59)	0.83(5)	0.430(50)	0.62(0.3)	n
95 BLG 32	18 00 49.9	-27 58 44	18.94	1.135(3)	1.180(8)	0.83(5)	0.600(50)	0.14(0.2)	y
96 BLG 16	18 01 09.0	-27 57 59	18.34	0.724(4)	0.906(5)	0.74(10)	0.44(10)	0.18(0.2)	y
95 BLG 38	17 59 41.9	-28 12 10	19.48	0.978(4)	0.980(24)	0.73(10)	0.50(10)	0.12(0.2)	y
95 BLG 21	17 59 42.1	-28 08 41	20.13	0.950(7)	0.890(39)	0.73(10)	0.41(10)	0.87(0.4)	y
95 BLG d3	18 00 35.6	-28 38 14	19.13	0.794(4)	0.789(14)	0.70(3)	0.339(40)	0.16(0.2)	n
97 BLG d2	18 00 39.6	-28 34 43	... <sup>a</sup>	... <sup>a</sup>	0.876(33)	0.70(3)	0.426(50)	0.95(0.2)	n
97 BLG d3	18 00 36.1	-28 32 34	18.38	0.932(5)	0.860(15)	0.67(4)	0.440(40)	0.78(0.2)	n
95 BLG d4	18 00 34.4	-28 33 30	19.92	0.798(7)	0.882(34)	0.67(4)	0.462(60)	0.90(0.2)	n
95 BLG d5	18 01 47.1	-28 21 26	19.28	0.845(5)	0.918(38)	0.71(3)	0.458(60)	0.11(0.3)	n
97 BLG d1	18 01 30.9	-28 32 16	19.62	0.981(5)	0.720(98)	0.75(8)	0.22(13)	0.89(0.4)	n
95 BLG 14	18 01 26.3	-28 31 14	17.67	0.904(2)	0.888(8)	0.75(8)	0.388(80)	0.06(0.2)	y

<sup>a</sup> No blue photometry available for this object

NOTE.—Col. (4) shows the V magnitude of the nearest Macho object. Cols. (5) and (6) show the colour from the PSF photometry and difference images respectively. Col. (7) gives the colour of the nearest RR Lyrae stars used for differential reddening correction. Col. (8) is the reddening corrected cousins colour. Col. (9) is the separation of the difference image centroid and the nearest photometered object. Col. (10) denotes whether the event was alerted on from the photometry. Cols. (4)–(8) include the  $1\sigma$  associated errors in the last one or two significant digits shown in parentheses.

TABLE 2  
PARAMETERS OF CLASSICAL EVENT FITS.

Event (1)	$t_{max}$ (2)	$A_{min}$ (3)	$\hat{t}_{min,d}$ (4)	$\hat{t}_{min,p}$ (5)	$\chi_d^2/N_{deg}$ (6)	$\chi_p^2/N_{deg}$ (7)	ErrR <sub>d</sub> % (8)	ErrR <sub>p</sub> % (9)	ErrB <sub>d</sub> % (10)	ErrB <sub>p</sub> % (11)
95 BLG 14	854.98(1)	4.23	19.3	18.5	0.91	0.46	1.12	2.18	1.97	2.97
95 BLG 21	902.47(7)	3.70	25.9	21.0	1.30	1.54	8.58	7.29	11.3	11.5
95 BLG 32	948.4(1)	2.40	65.8	68.7	2.22	1.03	1.51	1.78	4.73	3.98
95 BLG 33	970.48(19)	9.07	75.8	74.0	2.48	1.22	2.46	5.69	5.60	6.05
95 BLG 38	985.00(31)	2.35	85.4	76.5	1.25	2.15	4.27	8.19	7.04	8.05
96 BLG 16	1260.23(1)	7.78	90.0	83.3	2.96	0.93	2.69	7.76	4.43	6.85
95 BLG d3	956.4(8)	1.42	33.8	31.5	0.99	0.56	4.96	4.36	5.36	8.13
95 BLG d5	928.70(47)	1.52	18.2	24.2	0.48	0.87	3.83	4.56	6.07	6.21

NOTE.—Cols. (2) & (3) give difference image photometry microlensing fit values for amplification and  $t_0$  (microlensing time ( $JD - 2449000$ ) of closest approach), with the formal  $1\sigma$  fit error in the last one or two significant digits shown in parentheses. Cols. (4) to (7) give the minimum event time scale  $\hat{t}$  and  $\chi^2$  values obtained from fits to difference image photometry and PSF photometry. Cols. (8) to (11) give the median residual scatter of the photometry points about the fits for Blue and Red difference images ( $B_d$ ,  $R_d$ ) and PSF photometry ( $B_p$ ,  $R_p$ ). Fits assume PSF photometry baselines.

TABLE 3  
PARAMETERS OF PIXEL LENSING EVENT FITS.

Event (1)	$t_{max}$ (2)	$A_{min}$ (3)	$\hat{t}_{min}$ (4)	$\chi^2/N_{deg}$ (5)	ErrR <sub>d</sub> % (6)	ErrB <sub>d</sub> % (7)
97 BLG 51	1656.77(19)	3.58	74.1	1.41	22.9	31.3
95 BLG d2	982.9(1)	6.58	30.19	0.66	7.29	11.7
95 BLG d4	939.65(6)	3.14	10.34	1.04	8.61	18.6
96 BLG d1	1304.1(6)	1.91	59.3	0.93	4.22	8.74
97 BLG d1	1636.79(16)	2.11	10.5	0.84	7.65	13.5
97 BLG d3	1534.8(6)	2.38	35.53	1.05	9.59	14.5

NOTE.— Cols. (2) to (5) are difference image photometry microlensing fit values. Col. (2) gives the microlensing times (JD–2449000) of closest approach, with the formal  $1\sigma$  fit error in the last one or two significant digits shown in parentheses. Col. (3) presents the minimum amplification of the sources. Col. (4) gives the minimum event time scales. Col. (5) gives the reduced  $\chi^2$  values of the microlensing fits. Cols. (6) and (7) give the median residual scatter of the photometry points about the microlensing fits.

This figure "f1.gif" is available in "gif" format from:

<http://arxiv.org/ps/astro-ph/9903219v1>